frontiers | Frontiers in Water

TYPE Original Research
PUBLISHED 24 February 2026
DOI 10.3389/frwa.2025.1720178

OPEN ACCESS

EDITED BY
Rajesh Shrestha,
Environment and Climate Change Canada
Climate Research Division, Canada

REVIEWED BY
Moctar Diaw,
Cheikh Anta Diop University, Senegal
Ramanathan Alagappan,
Independent Researcher, Tiruchirapalli, India

*CORRESPONDENCE
Pranisha Pokhrel
✉ p.pokhrel@uu.nl

RECEIVED 07 October 2025
REVISED 13 December 2025
ACCEPTED 16 December 2025
PUBLISHED 24 February 2026

CITATION
Pokhrel P, Griffioen J, Bogaard TA, Kraaijenbrink PDA, Fiddes J and Immerzeel WW (2026) Upstream hydrology and the importance of snowmelt in buffering droughts in the Karnali basin in Nepal. *Front. Water* 7:1720178. doi: 10.3389/frwa.2025.1720178

Upstream hydrology and the importance of snowmelt in buffering droughts in the Karnali basin in Nepal

Pranisha Pokhrel[1]*, Jasper Griffioen[1,2], Thom A. Bogaard[3], Philip D. A. Kraaijenbrink[4], Joel Fiddes[5] and Walter W. Immerzeel[4]

[1]Copernicus Institute of Sustainable Development, Utrecht University, Utrecht, Netherlands, [2]TNO Geological Survey of the Netherlands, Utrecht, Netherlands, [3]Department Water Management, Delft University of Technology, Delft, Netherlands, [4]Department of Physical Geography, Utrecht University, Utrecht, Netherlands, [5]WSL Institute for Snow and Avalanche Research SLF, Davos, Switzerland

Understanding the hydrology in the upstream mountainous part of the Karnali basin in Nepal is vital, considering the importance of streamflow for downstream nature conservation and water supply. We use a fully distributed hydrological model to understand the current hydrology, the associated vulnerability of the basin, and the importance of the different hydrological components in regulating flow. Downscaled ERA5 meteorological data is used to force the model for the period 1991–2022 at a high spatial resolution (500 meters). We calibrate our model using observed discharges, and the model performance is considered good with a reported Kling-Gupta efficiency of 0.84 and a bias of −3.33%. Our results show that 40% of the overall discharge generated in the Karnali basin originates from rain runoff, 35% from baseflow, 24% from snowmelt, and a negligible 0.8% from glaciers. The water balance components vary spatially in magnitude, but the overall monthly patterns are comparable. On average, the basin receives 1,485 mm/year of precipitation, peaking in July, and is a pronounced southwest region. The annual average evapotranspiration in the basin is 574 mm/year, and discharge is 914 mm/year. Analysis of anomalies reveals that the discharge has become increasingly more variable over the last decades and, therefore, less predictable. Our results also reveal that the basin is frequently experiencing meteorological droughts, often translating into a hydrological drought with a lag time of a month. The average duration of a hydrological drought period in the basin was about 6 months. Snow storage plays an important role in modulating these droughts, and variability in initial snow storage impacts basin streamflow for up to 6 months. A climate change-induced shift from snow to rain may therefore impact the climate resilience of the Karnali considerably.

KEYWORDS

hydrological modeling, SPHY3.0 model, calibration and validation, Karnali basin, Nepal, discharge components, drought index, initial condition test

1 Introduction

Mountains are often called the water towers of the world and deliver an essential supply of water to the downstream regions, which are often densely populated, especially downstream of the Himalaya (Immerzeel et al., 2010; Viviroli et al., 2020, 2007). Snow and glacier melt from the mountains are major water sources and play a crucial role in the storage and constant

supply of streamflow, essential to meet both natural and anthropogenic water demands (Immerzeel et al., 2020). Understanding the hydrological drivers and the potential changes in mountain water supply is, therefore, of great scientific interest and societal relevance. Moreover, since mountainous river basins are vulnerable to climate change and are subjected to cryospheric changes, there is a high risk of extreme hydrological events (Calvin et al., 2023).

Most studies on hydrology and climate change in High Mountain Asia (HMA) have a near-continental scale and focus on the entire high mountain Asia region (Yoon et al., 2019; Khanal et al., 2021; Lalande et al., 2021) or are focused on very large river basins like the entire Indus (Lutz et al., 2014), Ganges (Raje et al., 2014), Brahmaputra (Pervez and Henebry, 2015), and the Yellow River basin (Wang et al., 2012; Zhang et al., 2022). At the other end of the spectrum, studies focus on a process-based understanding of small, high-altitude alpine catchments (Immerzeel et al., 2013; Ragettli et al., 2014, 2015, 2016; Buri et al., 2023). There is a large gap between large-scale studies and alpine catchment scale studies in High Mountain Asia. Yet, it is at this intermediate scale, which we define as medium-scale river basins, that the upstream-downstream linkages are most pronounced, where land use and water management decisions are made. There is, therefore, at this spatial scale, a strong need for medium-complexity, high-resolution hydrological models that can be used to assess the hydrological variability and the buffering capacity of the hydrological system to climate extremes and to quantify the impact of climate change and other factors like demographic development on water availability.

The Karnali River basin in Nepal is an example of such a medium-scale river basin (45,496 km^2). It is a perennial mountainous river basin in the Western region of Nepal that directly supports the domestic, agricultural, and industrial water needs of more than a million people in Nepal and India. The Karnali River basin is rich in biodiversity and supports four national parks, one wildlife reserve, one hunting reserve, and two buffer zones, and it is also a habitat for endangered species (Khatiwada and Pandey, 2019) all of which rely on natural river dynamics. The Karnali River is characterized by steep slopes and high discharge and stands as Nepal's largest remaining mostly undisturbed river. Given the basin's high potential for hydropower, the national interest in harnessing this potential for development and economic growth, and the basin's ecological value, understanding the present-day hydrology at high spatial detail is crucial. Such a baseline is required to understand the streamflow composition and the sensitivity to future changes related to climate and land use change.

A few studies have been conducted in the Karnali basin to understand the region's hydrology and vulnerability to climate change. Pandey et al. (2019) surveyed 3,660 local households located in the Karnali and Mahakali River basin (which borders the Karnali River basin in the west), and reported that 79% of the households are experiencing extreme and irregular weather events like droughts, heavy rainfall, and floods with significant impact on the livelihoods of the mountain communities. Khatiwada and Pandey (2019) characterized the occurrence of major drought events in the Karnali basin and reported an increase in the frequency of drought for the monsoon season (June to September) from 1981 to 2014. A study by Khatiwada et al. (2016) analysed meteorological station data to understand the long-term climatic trends of the basin. Their findings revealed declining precipitation and rising temperature during the study period (1981–2012), signaling a shifting climate regime. In a related approach, some studies focused on historical recorded discharge data and showed that discharge does not depict any significant trend but was subjected to interannual variability (Khatiwada et al., 2016; Dahal et al., 2020; Hasan and Pradhanang, 2017). Hasan and Pradhanang (2017) demonstrated a strong interlinkage between river discharge and groundwater flow, and concluded groundwater flow was declining, particularly during the monsoon season (June to September) in the study period (1979–2007). Various studies using semi-distributed models advanced our understanding of the water balance components and vulnerability to climate change in the Karnali River basin and major sub-basins (Hasan and Pradhanang, 2017; Dhami et al., 2018; Pandey et al., 2019, 2020a,b; Dahal et al., 2020; Pradhananga et al., 2025). These studies provided a base for understanding the hydroclimatic dynamics of the Karnali River basin. However, key limitations exist, notably: (a) reliance on short and discontinuous ground-based data records of the existing network, which is mostly clustered at lower elevations of the basin (< 2,000 m above mean sea level), and (b) the modelling approaches are generally based on lumped models. On the contrary, a distributed model would help to improve our understanding of regional differences in water availability by using a gridded dataset to better represent the heterogeneous characteristics, along with glaciers and snow processes that are important for the water balance in the basin.

In this study, we bridge the gap in scale between hydrological studies that focus on the entire high-mountain Asia and small-scale catchment studies at high altitudes by studying the medium-scale Karnali River basin. We aim to fill the research process gap for the Karnali River basin study by using a distributed model to simulate the hydrological processes in the basin at a high resolution to quantify a benchmark water balance, assess hydrological shifts, and evaluate drought response in the Karnali River basin. For this, we use the Spatial Processes in Hydrology (SPHY) model (Terink et al., 2015), which represents snow and glacier processes at an intermediate level of detail. We used SPHY version 3.0; the source code is freely available with installation guidelines (FutureWater, 2019; Khanal et al., 2024). The application of SPHY in the Karnali River basin improves the spatial representation of hydrological parameters with a focus on the snow properties that are important for water balance in the basin. Using the calibrated model, we first analyze present-day hydrology using seasonal water balances and the spatial distribution of flow components. Second, we investigate anomalies in the discharge of the basin and analyze the severity of these anomalies using drought indices. We hypothesize that winter snowfall and associated spring snow storage in the basin have a critical role in buffering against droughts. Therefore, in the next step, we focus on the propagation of meteorological drought to hydrological droughts and explore whether snow storage plays a role in altering the onset and recovery of the hydrological droughts. Finally, we explore how long snow storage could buffer hydrological droughts at different elevations.

2 Study area

The Karnali River is one of the three most prominent rivers in Nepal, along with the Koshi and Gandaki Rivers. The Karnali River originates from the Tibetan Plateau and the Himalayan mountains in

the north, flowing through hills and valleys to the plains of the Terai in the south. The river basin extends between 80.52° to 83.78° E and 28.19° to 30.72° N and covers an area of 45,496 km^2 upstream of Chisapani (Figure 1). About 93% of the total basin area falls within Nepal, and the remaining area is located on the Tibetan plateau in China. Downstream of Chisapani, the Karnali River exits the foothills and enters the plains, where the main river branches off and deposits the sediment over a large area, known as "Karnali Megafan." The elevation in the basin ranges from 186 to 7,606 m above mean sea level, with an average elevation of 3,307 m. The river receives water from snow and rain-fed tributaries. The Humla Karnali, Mugu Karnali, and Tila Rivers converge in the north and form the main stem of the Upper Karnali River. The West Seti River, with a basin area of 7,378 km^2, is the major tributary that originates in the Himalayas on the far western side and confluences with the Karnali in the south. The Bheri River, with a basin area of 13,450 km^2, is another major tributary on the eastern side that also joins the Karnali River in the south. The Karnali River at Chisapani receives about 22 and 27% of its total discharge from the West Seti and Bheri Rivers, respectively.

The river basin's precipitation patterns are influenced by both monsoon precipitation originating from the Indian Ocean and winter precipitation associated with the Westerlies. In comparison to other regions of Nepal, western Nepal is relatively dry. The precipitation in the basin occurs over four climatic seasons and is marked by high spatial variability. About 77% of the total precipitation falls during the summer monsoon season between June and September, and only 7% falls in winter (Khatiwada and Pandey, 2019). The influence of the monsoon precipitation decreases towards the northwest, and this sub-area is the driest part of the basin (Dahal et al., 2020).

The river basin shows high variability in temperatures due to the large elevation differences, with the extremes as high as 40 °C in the southern lowlands during summer and dropping to −14 °C in the northern high-altitude mountains during winter (Khatiwada and Pandey, 2019). The upper region of the basin is mostly dominated by grassland, sparse vegetation, and snow/glaciers. In total, 32% of the basin area is covered by Grassland (Figure 2). The lower region of the basin is characterized by various types of forests, croplands, urban areas, and some grasslands. In total, 48% of the total area is classified as trees (Figure 2).

To discuss spatial variations in hydrometeorological parameters in this study, we will be using basin definitions: "Karnali basin overall", which refers to the entire upstream Karnali River basin above Chisapani; "Upper Karnali basin", which refers to the sub-basin with the main stem of Karnali before it merges with Bheri or West Seti River; "Bheri sub-basin," and West Seti

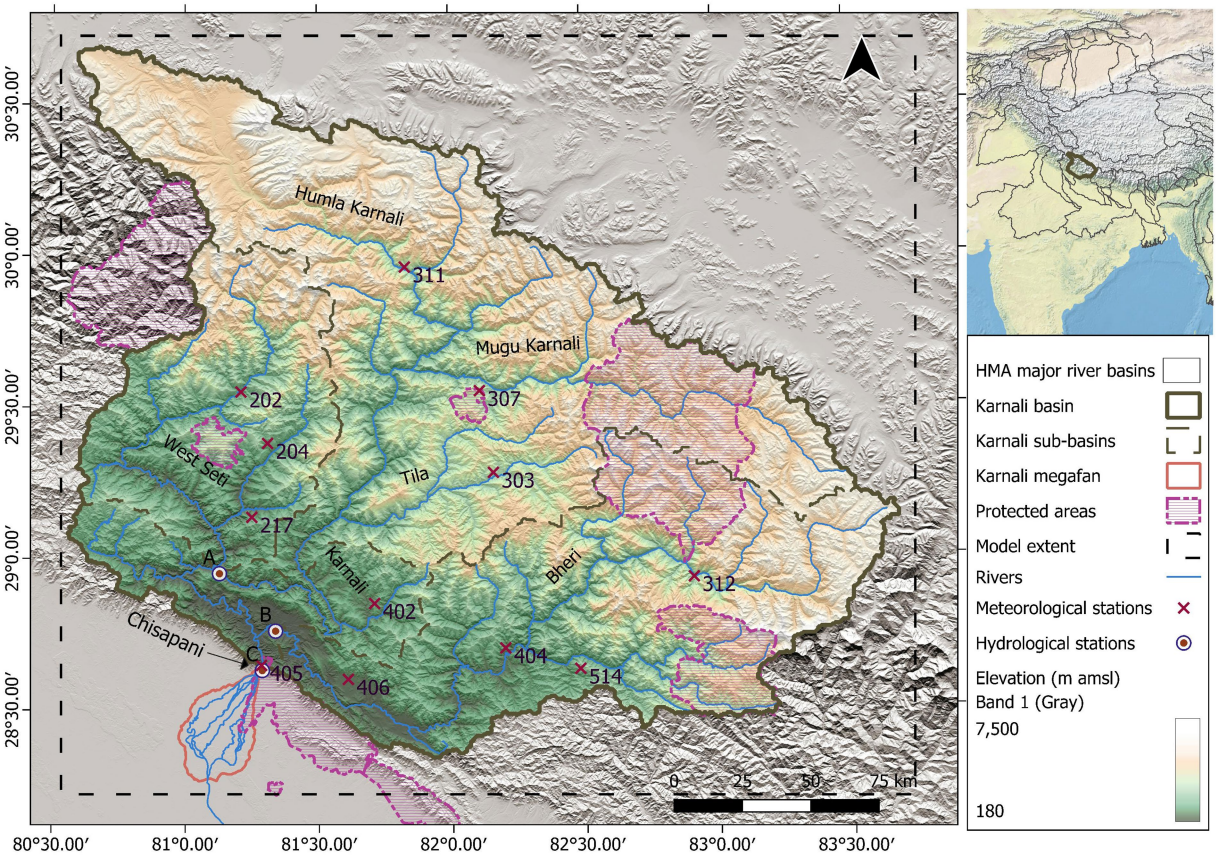

FIGURE 1
Topographical map of the Karnali basin, overall showing the locations of the hydrological stations used for calibration and validation. The meteorological stations used to compare forcing data with ground stations are marked. Protected natural conservation areas within the Karnali basin are also highlighted, sourced from Protected Planet (UNEP-WCMC, 2026). The High Himalaya major river basins are from the ICIMOD repository (ICIMOD, 2021). Background imagery in the key location map is from Nature Earth, accessed February 2026 (https://www.naturalearthdata.com/).

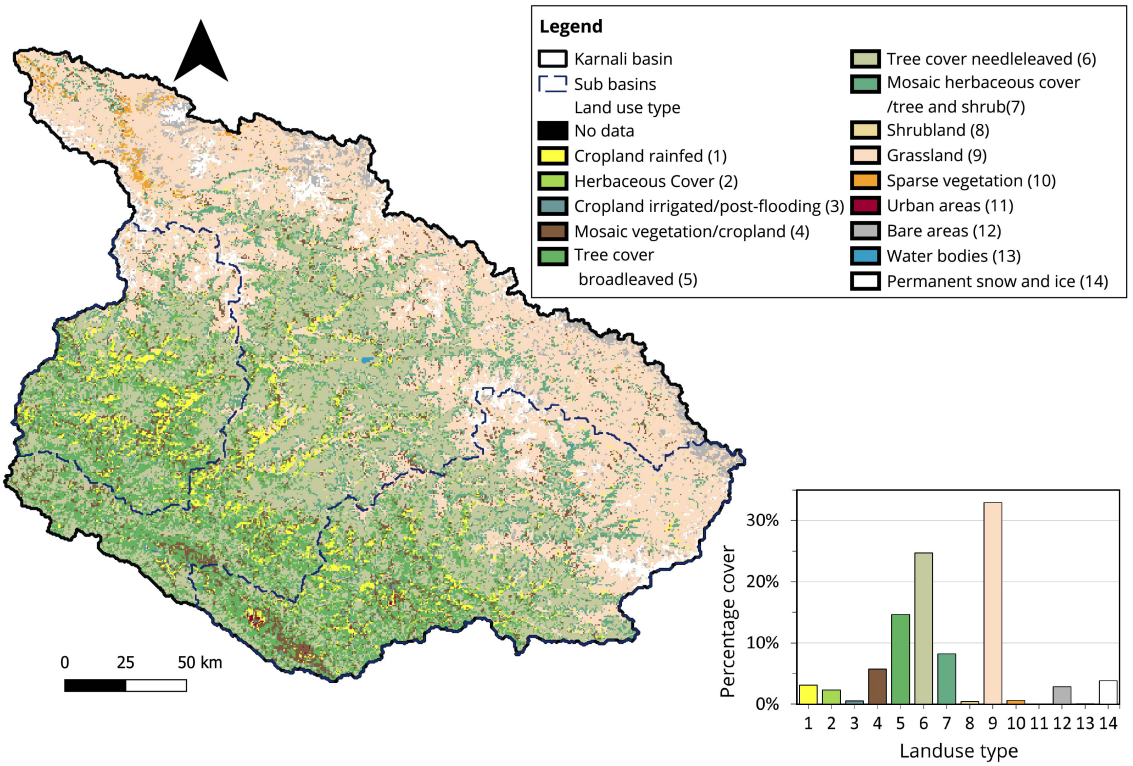

FIGURE 2
The land cover map for the entire Karnali basin overall area was reclassified to highlight the classes relevant to the study. Source: Modified from Copernicus Climate Change Service (2019). Used under CC BY license.

sub-basin," referring to the Bheri and West Seti River sub-basins, respectively.

3 Methodology

3.1 Model

SPHY is a fully distributed, raster-based "leaky-bucket" water balance model. It includes snow and glacier modules and simulates rainfall runoff, snow and glacier melt, evapotranspiration, and soil hydrological processes. SPHY model has been applied in research across large mountainous river basins like the Indus, Ganges, and Brahmaputra (e.g., Lutz et al., 2016; Wijngaard et al., 2018, 2017) as well as to the entire HMA (e.g., Khanal et al., 2021). The model has also been used and validated for small basins like the Tamor River basin (Pradhan et al., 2024), Chameliya River basin (Nepal et al., 2024), and Chandra-Bhaga basin (Srivastava et al., 2024), demonstrating the capacity to simulate hydrology at diverse scales. In this study, we extended the application of SPHY to an intermediate-scale basin. We set up the SPHY model with a spatial resolution of 500 × 500 m and a daily temporal resolution. The model covers an area of 86,758 km^2 and was run for a period of 32 years from 1991 to 2022 with a daily timestep. The resolution selected is a compromise between the processing time and the level of detail that we want to achieve.

SPHY requires a daily time series of precipitation and minimum, maximum, and average temperature as climate forcing. The SPHY model generates the total simulated discharge (Q_{Tot}) as well as its components. Q_{Tot} can be expressed as in Equation 1.

$$Q_{Tot} = Q_{RR} + Q_{SM} + Q_{GM} + Q_{BF} \quad (1)$$

Q_{RR} is the total discharge generated due to surface runoff and lateral flow from the soil water storage. Q_{SM} is the snowmelt discharge component and is calculated using a degree-day model. The model also accounts for the refreezing of meltwater, and the snowmelt discharge component will only be generated when the snowpack is saturated. The limitation of snow module in SPHY V3.0 is that the melt water from the snow is directly routed to the river network and does not percolate into the ground. Q_{GM} is the glacier melt discharge component, and it is calculated using a degree day model, with different degree day factors for clean ice and debris-covered glaciers. The glacier model in SPHY is mass-conserving, and snow accumulating in the accumulation area is transported to the ablation area annually through a simple ice dynamics model. Glacier melt can either contribute to the total discharge as direct flow or percolation into groundwater based on a user-defined parameter. Soil water processes in the SPHY model happen in three soil layers: the root zone, the sub-zone, and the groundwater layer. Q_{BF} is the baseflow component from the groundwater layer, which is generated when the groundwater storage exceeds a user-defined threshold. The soil water content is controlled by evapotranspiration, infiltration, and capillary rise from the groundwater. If the soil water content is above field capacity, percolation to groundwater occurs. Q_{Tot} is the summation of all the cell-specific flow components, which is then routed using a routing scheme and flow direction network.

In the following paragraph of this research paper, we look into the distribution of these flow components, where rain runoff, snowmelt, and glacier melt are the direct flow components, and baseflow is the indirect flow component to the discharge of the river.

3.2 Data

We used the ALOS Global Digital Surface Model (AW3D30) (Japan Aerospace Exploration Agency, 2021) of 30 m resolution as a digital elevation model (DEM). We resampled the DEM into the model resolution of 500 m and corrected the DEM for sinks. We then determined the slope and direction of drainage for model inputs. We used ERA5 reanalysis (Hersbach et al., 2020), which is the fifth-generation European Centre for Medium-Range Weather Forecasts (ECMWF) atmospheric global climate reanalysis data as meteorological forcing for the model. Hourly ERA5 data for the period 1991–2022 were bias-corrected (relative to elevation) and downscaled to model resolution using TopoPyScale (Fiddes and Gruber, 2014; Filhol et al., 2023) and then aggregated to the daily fields required by the SPHY model. We then applied gridded daily precipitation and temperature (minimum, maximum, and average) fields as forcing for the model.

We based the glacier outline for the model using Randolph Glacier Inventory 6 (RGI6) (Pfeffer et al., 2014; RGI Consortium, 2017). We computed the glacier fraction (debris-covered and clean ice) for each 500 m resolution grid cell (Kraaijenbrink et al., 2017). We referenced the thickness and mean elevation of the glacier grid cells from Farinotti et al. (2019).

The land cover data for the model is based on existing land cover series produced under the European Space Agency's Climate Change Initiative (ESA CCI) (Defourny et al., 2023). The land cover map dataset has a 300 m spatial resolution and 22 classes (available at http://maps.elie.ucl.ac.be/CCI/viewer/download.php, last access: 23 Jan 2023). We resampled land cover data into the model resolution and reclassified it into 14 broader classes based on the cover type and coverage. We derived the crop coefficient (k_c) values for each land cover type from Allen et al. (1998).

We collected the root zone and subzone soil hydraulic properties for the model from the global HiHydroSoil v2.0 database (Simons et al., 2020). The database contains maps for hydraulic properties such as saturated hydraulic conductivity, water content at field capacity, and critical and permanent wilting point at 250 m resolution, all of which we resampled to the model resolution. The model input also requires a depth of soil in the root-zone and sub-zone. We considered these depths as the parameters for calibration. We also parameterized root depth as a slope-dependent variable with a maximum depth at slopes of 0 degrees and a minimum depth for the slopes of 45 degrees or more (see parameter "RootDepthFlat" in Table 1) and varied them per basin.

In-situ hydrological and meteorological data at daily temporal resolution in the river basin are available from the Department of Hydrology and Meteorology of Nepal (DHM Nepal). We collected hydrological data from three stations for the calibration process (see Figure 1 for station locations). The stations are:

1) Station no. 260 for the Seti basin, located near the Seti-Karnali confluence and labeled as (A) in the Figure 1;

TABLE 1 Parameters selected for sensitivity and their final value in the model.

Parameter	Definition	Unit	Base value	Final value		
				Seti sub-basin	Bheri sub-basin	Karnali basin overall
α_{gw}	Baseflow recession coefficient (range 0.1–1.0)	-	0.3	0.3	0.4	0.5
kx	Flow recession coefficient	-	0.9	0.85	0.94	0.89
δgw	Delay in groundwater recharge	Days	70	49	123	60
DDFS	Snow degree day factor	mm degree^{-1} day^{-1}	4.5	4	4	4
Tcrit	Critical temperature for precipitation to fall as snow	Degrees Celsius	0	2	2	2
RootDepthFlat	Thickness of rootzone	mm	450 (varying with slope with max value for slope 0)	265	390	400
CapRiseMax	Maximum capillary rise from subsoil to the rootzone	mm day^{-1}	3	0.01	0.01	0.01
CropFac	Lookup table with crop coefficient for each landuse ID	-	0% (as % change to base value)	−30%	−8%	−15%
BaseThresh	The minimum value for baseflow to occur	mm	5	0	10	10

2) Station no. 270 for the Bheri basin, located near the Bheri-Karnali confluence and labeled as (B) in the Figure 1; and
3) Station no. 280 for the Karnali basin, situated at the outlet Chisapani of the overall study area and labeled as (C) in the Figure 1.

The hydrological data for stations A and C were available up to 2019; for station B, the data were only available until 2016. Additionally, we gathered recorded meteorological data from 10 stations within the basin. We compared the long-term observed precipitation and temperature data to the downscaled ERA5 data. The comparison of the average monthly temperature data is shown in Supplementary Figures A.3, A.4. The locations of these observation stations are shown in Figure 1. We further corrected the differences in the temperature (minimum, maximum, and average) between recorded and downscaled ERA5 data using the mean bias correction method and using an average correction factor. Precipitation data was not corrected.

3.3 Model parameterization and performance

The initial model parameters were based on previous work by Khanal et al. (2021). Subsequently, we performed a sensitivity analysis to quantify the sensitivity of the parameters on simulated discharge at the river basin outlet. This analysis involved systematically varying the parameters by pre-defined percentages (e.g., ±5 to ±75%) and evaluating the resulting change in discharge components. We iteratively adjusted the parameter value using the results from the sensitivity analysis and compared simulated daily discharge with measured discharge at three different locations. The daily discharge measured at Bheri station consisted of 50% missing data for the years 2014–2016; therefore, the calibration period for the model was selected from 2003 to 2013.

We validated the model parameters for the period 1991–2001. We used several metrics: percentage bias (PBIAS), Nash-Sutcliffe efficiency (NSE) (Nash and Sutcliffe, 1970), coefficient of determination (R^2), and Kling–Gupta efficiency (KGE) (Gupta et al., 2009) to evaluate the model's performance. The parameters selected for the sensitivity analysis and their final calibrated values are given in Table 1.

3.4 Hydrological analysis

3.4.1 Discharge composition and trend

After the model was calibrated, we looked into discharge composition to understand the seasonal flow dynamics and the drivers of the flow. We investigated the water balance components and the spatial variations of these components in the basin. Direct simulation of individual runoff components in SPHY removes the need for empirical baseflow separation and improves understanding of hydrology compared to semi-distributed model approaches. We also assessed long-term changes and examined monthly anomalies in the historical discharge to check the above-average and below-average flow signals. Persistent anomalies indicate the irregularities in the flow and a shift in seasonality.

3.4.2 Correction of snow storage

Snow storage follows a seasonal cycle each year, where we observe a natural rise during winter due to higher amounts of snowfall and a fall in the summer due to higher melt. The snow module in SPHY simulates key processes, such as accumulation, melting, refreezing, and storage. However, SPHY has a temperature-based melt model, and it does not simulate all ablation processes like sublimation, wind-driven, and gravity-driven transports. Therefore, at high elevations where low temperatures limit melt, snow storage can accumulate unrealistically over time for some grid cells. This undermines the ability to assess the role of snow storage during droughts, as it skews any domain-wide statistics calculated of the snow storage. To correct the small fraction of cells showing this behavior (0.9% of the model domain), we removed the year-to-year increase in annual minimum SWE. To do this, we linearly interpolated the modeled snow storage on 30 September of each year (lowest annual SWE) to a daily series that represents the unrealistic trend. This interpolated timeseries is then subtracted from the full 32-year timeseries. This approach preserves the intra-annual variability in snow storage while eliminating the erroneous long-term increasing trend. Because this correction was applied after the hydrological model run, it did not alter any other model processes or routing that produced the simulated discharge.

3.4.3 Drought analysis

We characterized meteorological droughts using the Standardized Precipitation Evapotranspiration Index (SPEI) developed by Vicente-Serrano et al. (2010) and hydrological droughts using the Standardized Streamflow Index (SSI) (Modarres, 2007; Vicente-Serrano et al., 2012). Both indices were calculated to see if a meteorological drought propagates into a hydrological drought. SPEI is based on the normalization of the difference between precipitation and potential evapotranspiration. The SSI is based on the normalization of the discharge time series (Vicente-Serrano et al., 2010). We used simulated discharge data, potential evapotranspiration, and downscaled ERA5 precipitation data to calculate these drought indices. We calculated SPEI using a log-logistic distribution and SSI using a gamma distribution. We then cross-correlate the SPEI against the SSI values for different aggregation periods to identify the time interval at which the river discharge is most strongly correlated to the meteorological conditions. Cross-correlation analysis was also used to assess the lag between the SPEI and the SSI. We then followed the standard drought classification based on the index values following McKee et al. (1993), which classifies an event as a drought if the index in that period is negative. If an index is between 0.00 and −0.99, it is classified as a mild drought; between −1.00 and −1.49, it is a moderate drought; between −1.50 and −1.99, it is a severe drought; and ≤ 2.00, it is considered an extreme drought. In a final step, we focused on two extreme drought events and investigated the role that snow storage and melt have played in mitigating the drought.

Understanding the propagation of hydrological drought is more complex, especially in the basins influenced by seasonality and factors like the presence of snow, glaciers, and fluctuating soil moisture (Peña-Gallardo et al., 2019; Van Loon et al., 2014), along with the meteorological conditions. Therefore, we assessed the importance of initial snow storage, baseflow, and soil moisture in buffering droughts following a similar approach as Wanders et al. (2019). We selected a year with average hydrological conditions from the 1991–2022 time series. Next, we ran the selected year 32 times from 1 March to 28 February. We started the runs on 1 March as snow storage peaks at the end of February. For each run, we varied the initial conditions of snow

storage, base flow, soil moisture, and meteorological forcing. These initial conditions were derived from the transient 32-year run. We then used this set of simulations to compute the variance in discharge attributed to the initial conditions as a function of the lead time. In other words, we assess for how long streamflow is influenced by the initial snow storage, baseflow, or soil moisture status.

The results from the initial condition test can show how the modelled discharge is impacted by the initial condition of the different state variables. With this analysis, the importance and different timescales of the initial hydrological storage on buffering droughts can be established. We selected several outlet locations at various elevations to assess the spatial differences and variability due to changes in initial conditions.

4 Results and discussions

4.1 Model performance

We evaluated the calibration by comparing simulated and observed discharge for the three main outlets: A. near the confluence of the West Seti and the Karnali, B. near the confluence of the Bheri and the Karnali, and C. the overall Karnali, after convergence of the other two rivers. The location of the stations used for the comparison is given in Figure 1. Figure 3 shows the simulated daily discharge, along with its components, compared to the observed discharge for the calibration period. We used multiple metrics to evaluate the accuracy of the simulated discharge (see Table 2). The KGE for the calibration period was 0.82 for West Seti, 0.84 for Bheri, and 0.79 for the overall Karnali. The NSE was 0.66 for West Seti, 0.73 for Bheri, and 0.80 for the overall Karnali. Both metrics demonstrated good model performance and indicated accuracy in simulating the flow. The PBIAS of 10.7% in the Bheri basin suggested the overestimation of the discharge in the basin. The positive discharge bias of 10% during the calibration period could be explained by a potential positive bias in the ERA5 precipitation. The positive bias has been reported in previous studies (Khanal et al., 2021, 2023; Lavers et al., 2022). The overestimation of precipitation also shows in the comparison of the long-term monthly precipitation from ERA5 with the station data (see Supplementary Figure A.2A). Stations at higher elevations, such as 303, 307, 311, and 312, has positive biases of more than 50%. However,

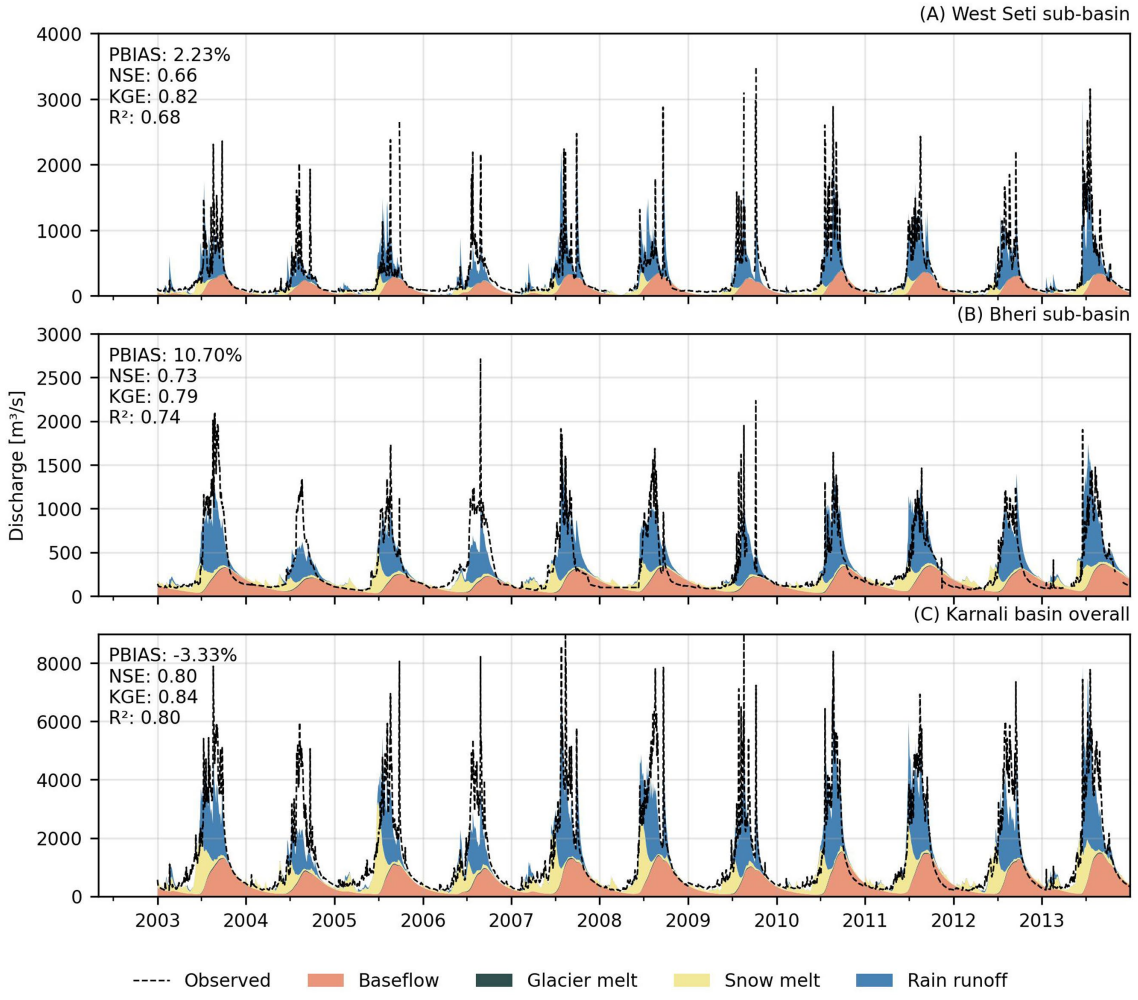

FIGURE 3
Hydrographs of daily observed and simulated discharge for the calibration period (2003–2013) for the two main sub-basin outlets and Karnali basin as a whole, with an outlet at Chisapani. The simulated discharge components are stacked.

TABLE 2 Model performance metrics for the calibration and validation period using daily discharge data.

Period	Metrics (daily)	West Seti sub-basin	Bheri sub-basin	Karnali basin overall
Calibration period (2003–2013)	PBIAS	2.30	10.80	−3.40
	NSE	0.66	0.73	0.80
	R^2	0.66	0.73	0.80
	KGE	0.82	0.79	0.84
Validation period (1991–2001)	PBIAS	1.10	−5.50	−8.90
	NSE	0.66	0.76	0.76
	R^2	0.66	0.76	0.76
	KGE	0.82	0.66	0.78

TABLE 3 Probability of exceedance value in [m^3/s] at $Q_{10\%}$, $Q_{50\%}$, and $Q_{90\%}$ for three outlets in the West Seti sub-basin, the Bheri sub-basin, and the overall Karnali basin. The terms "Obs" and "Sim" in the table are short for simulated and observed discharge data, respectively.

Basin and Period	Scenario	$Q_{10\%}$	$Q_{50\%}$	$Q_{90\%}$
West Seti sub-basin	Sim	794	124	35
	Obs	784	114	69
Bheri sub-baisn	Sim	823	222	113
	Obs	937	161	87
Karnali basin overall	Sim	3,329	678	264
	Obs	3,750	670	276

The terms "Obs" and "Sim" in the table are short for simulated and observed discharge data, respectively.

these stations have considerable amounts of missing data (see Supplementary Figure A.2C) and usually are affected by precipitation under catch since part of the precipitation falls as snow. Overall, the Karnali basin receives, on average, 1,485 mm/year of precipitation based on ERA5 forcing. This amount aligns closely with the findings from earlier work: 1,479 mm/year for the period 1981–2012 by Khatiwada et al. (2016), 1,239 mm/year for the period 2000–2015 by Khatakho et al. (2021) and 1,437 mm/year for period 2000–2010 by Pradhananga et al. (2025). While periods analyzed are different between the studies, the consistent multi-year average precipitation shows the ERA5 dataset is suitable for forcing our long-term hydrological model study. Furthermore, the comparison with the station data shows the seasonality is capture well, and we do not observe a significant bias in discharge during the validation period (Table 2). We observed negative PBIAS of −5.5% and −9.0% in the Bheri sub-basin and Karnali overall for the validation period. In some cases, the model fails to capture the occurrence of peak flow events (see Figure 3). The negative biases and differences encountered in the simulated and observed discharges can be associated with both the limitations in the model and the inaccuracies in the forcing to represent extreme events.

We also compared the distribution of the flow between simulated and observed data by calculating the discharge value at different exceedance probabilities in Table 3. The discharge value at outlets shows that the entire flow distribution was well reproduced by the calibrated model, with acceptable differences. In the Karnali River at Chisapani outlet, we calculated 3,329 m^3/s as the simulated discharge corresponding to an exceedance probability of 10%, which is slightly less than the observed discharge value of 3,750 m^3/s. Likewise, at the outlet of the Bheri sub-basin, discharge corresponding to a 90% exceedance probability was 113 m^3/s, which is higher than the value of 87 m^3/s obtained from the observed discharge series. The simulated long-term average flow in the Karnali basin for the model period 1991–2019 was 1,291 m^3/s, which closely matches the observed flow of 1,356 m^3/s during the record period of 1991–2019. Therefore, we concluded that the overall model performance is satisfactory.

While the model reproduces hydrological patterns, there are some limitations of the study. The SPHY model uses a relatively simple routing scheme that only considers the recession coefficient and water accumulation from one cell to a downstream cell to calculate the total flow. The model also uses a stationary recession coefficient to characterize baseflow, which does not vary in space or time. The use of advanced routing schemes, such as diffusive wave routing or even fully dynamic routing, would better simulate the flow, especially the peaks, but they come with large data requirements and computational time, which was not feasible for this scale of study. The coarse spatial resolution of the ERA5 data (31 km) does not fully capture the high spatial variability of precipitation in the mountainous parts of the Karnali basin. In addition, the clustering algorithm that is used in the downscaling process also has an associated uncertainty that may, in rare cases, result in misclassified pixels. These errors are also difficult to further rectify with station data, as the network is sparse and about 90% of the stations are concentrated on the lower elevations (< 3,000 m). We have calibrated the model using three stations representative for the three major tributaries Karnali, Seti and Bheri. These stations are located downstream so they represent the full sub-basin hydrology and we calibrate model parameters per sub-basin. However, to better constrain cryospheric model parameters we do recommend for future studies also to include upstream discharge stations. Especially since the observational network is currently being expanded and improved by the Department of Hydrology and Meteorology in Nepal.

4.2 The Karnali water balance

The long-term monthly water balance components spatially (Figure 4) demonstrated a comparable seasonal pattern over the entire Karnali basin and its sub-basins in the east and the west. Overall, the Karnali basin received the maximum amount of precipitation from June to September, during the monsoon season, with a peak value in July (365 mm/month). The actual evapotranspiration (ET) in the overall basin also peaked in July (96 mm/month) when water availability and air temperature were high. On average, the basin experienced an annual ET of 574 mm/year which is about 39% of precipitation, consistent to the estimates by Pradhananga et al. (2025) and Pandey et al. (2020a). The southwest region was the wettest of the basin. Most of the precipitation fell in the elevation range between 1,000–2,000 m, mostly on the southern side of the Himalayas, and the northern part of the basin, located in the rain shadow of the main Himalaya range, is driest (Figure 5A). The spatial distribution of ET (Figure 5B) generally coincided with the precipitation pattern, peaking

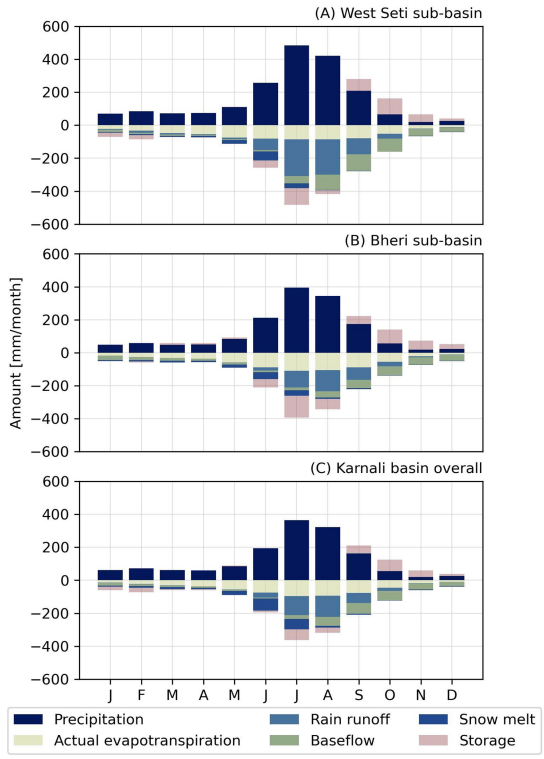

FIGURE 4
Monthly water balance components for **(A)** the West Seti sub-basin, **(B)** the Bheri sub-basin, and **(C)** the overall Karnali basin.

in the southern parts, dominated by forest and agricultural lands with adequate rainfall. ET was lowest in the north, where temperatures were low and land cover was either barren, sparsely vegetated, grasslands, or permanent snow.

The long-term monthly water balance components in Figure 4 indicate that the discharge was primarily driven by rainfall during the monsoon period from June until September, by baseflow between October and January, and by snowmelt between February and June. While the seasonal patterns between the sub-basins in the east and west were comparable, spatial heterogeneity in the magnitude existed due to topographical and climatic differences. Rainfall runoff was generated mostly from the hills and lowland regions, with the highest value of 1,527 mm/year in the south-western part (Figure 5C), which aligns with the higher amount of precipitation received in this region due to the influence of both monsoon winds and occasional precipitation by westerlies. The West Seti basin received an average rain runoff of 224 mm/month in July due to monsoon precipitation and 11 mm/month in February due to winter precipitation from the Westerlies (Figure 4A). The runoff coefficient in the West Seti River sub-basin was 36%, which is higher compared to the Bheri River sub-basin in the east (24%), indicating that the western region of the basin has higher drainage capacity than the rest of the basin. The baseflow component was also higher in the West Seti basin compared to the other parts of the overall Karnali basin, with a maximum value of 102 mm/month during September. Overall, the water balance highlights that the monsoon precipitation is the primary hydrological driver in the Karnali basin, which has also been highlighted in the study by Pandey et al. (2020a).

On average, the Karnali basin received discharge of 223 mm/year from snowmelt for the historical period. The discharge from snowmelt was seasonally variable, which began in the winter, peaked in early summer, and declined in late summer to autumn. With an increase in the snowmelt value from 6 mm/month in January to a peak value of 74 mm/month in June (Figure 4C), the percentage of snowmelt contribution relative to the monthly average discharge ranged from 26% (in January) to 74% (in May) in the overall Karnali basin. This suggests that the snowmelt contribution plays a substantial role in the water availability in the basin during the spring and early summer period. The snowmelt sharply declined during late summer when the snow storage was depleted. The seasonal pattern of the snowmelt was similar across the sub-basins, but the magnitude differed spatially (Figure 5D).

On average, the discharge at the outlet point at Chisapani originated from about 28% from the Bheri sub-basin, 22% from the West Seti sub-basin, and the remaining 50% from the regions of the Upper Karnali basin, with contributions from snow-fed tributaries like Mugu Karnali, Humla Karnali, and Tila Karnali rivers. The contributions of snowmelt, glacier melt, rainfall runoff, and baseflow to the total discharge varied between the sub-basins (Figure 5F). For the model period from 1991 to 2022, 40% of the total discharge at the outlet Chisapani in the Karnali basin was primarily due to rainfall runoff, indicating that the Karnali basin is predominantly rain-dominated. Baseflow was the second largest component, contributing 35% of the total discharge in the overall Karnali basin, which was comparable between the sub-basins. Discharge from snowmelt contributed, on average, about 24% to the total discharge for the overall Karnali basin which was slightly higher than an average of 15% as reported by Dhami et al. (2018) using a semi-distributed model. Higher melt percentages simulated from SPHY could be due to its advantage of calculating melt at grid cell level and also allowing fractional coverage in cells separating glaciers and snow. The snowmelt contribution was higher for the Bheri sub-basin (18%) than for the West Seti sub-basin (11%). Most of the snowmelt was generated in the higher reaches of the Upper Karnali basin region. This can be explained by the basin hypsometry, and only 32% of the total surface area of the West Seti basin is above 3,000 m (Supplementary Table A.1), 59% for the Bheri sub-basin and 62% for the overall Karnali basin. Glacier melt only contributes marginally to the total discharge (0.8%) since glaciers only cover 2% of the total basin area.

Figure 5E shows a heat map of the monthly average rainfall runoff, and snowmelt by elevation. Most of the rainfall-generated discharge is logically generated during the monsoon (JJAS) and predominantly from elevations below 4,000 m. The snowmelt-generated seasonal discharge originates from different elevation bands depending on the month. The snow accumulated below 5,000 m drives winter (JFM) and pre-monsoon season (AM) discharge, and snow accumulated above 5,000 m largely contributes to discharge during the monsoon (JJAS) (Figure 5E). This emphasizes the importance of winter snow accumulation at different elevations in sustaining the flow in subsequent months. Climate change is likely to impact the snow accumulation and melt in future (Gobiet et al., 2014; Musselman et al., 2017; Ishida et al., 2019; Kraaijenbrink et al., 2021, 2017). A warming climate will induce a phase shift from snowfall to rainfall leading to elevation dependent changes in both magnitude and timing of snowmelt contribution. Because seasonal snowmelt governs the runoff timing of the basin (Armstrong et al., 2019), combined changes in snow accumulation, melt timing and rates can considerably alter the

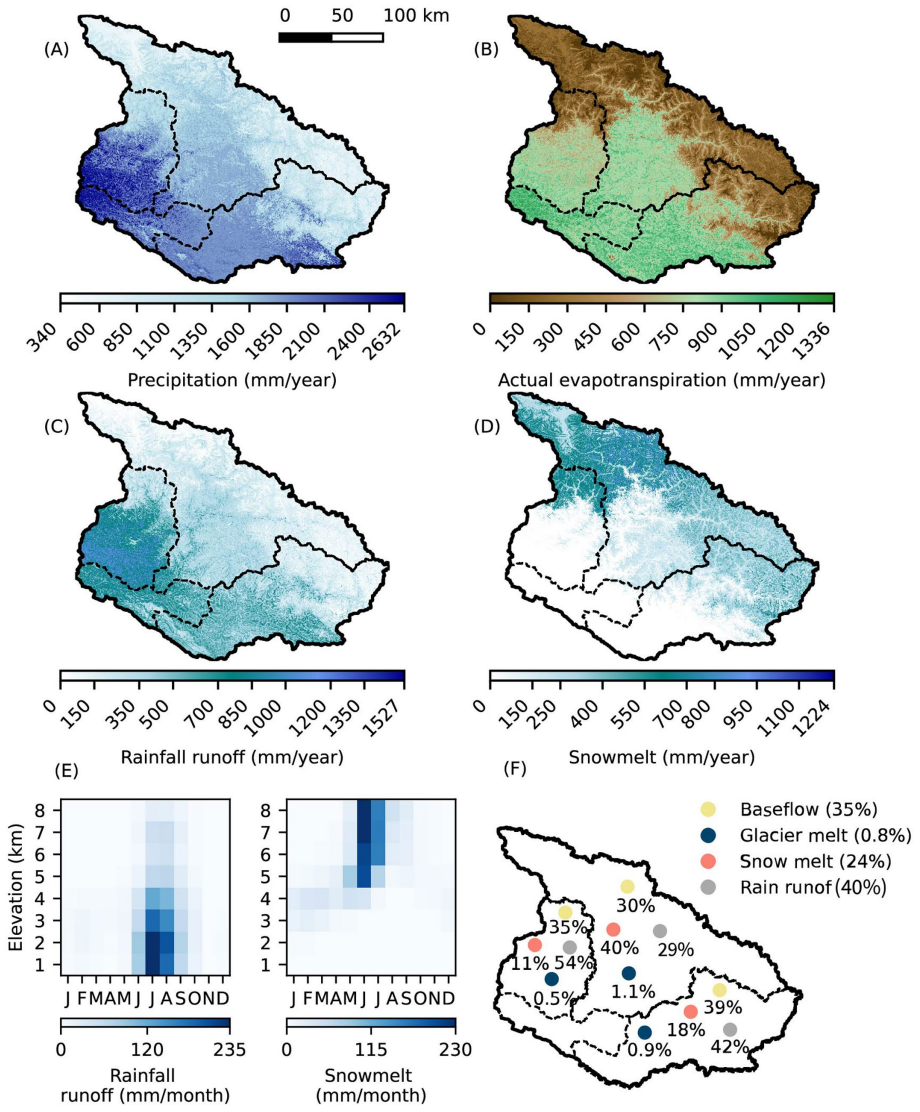

FIGURE 5
Spatial maps for annual averages of different water balance components for the overall model period (1991–2022) in the Karnali basin overall: **(A)** Precipitation, **(B)** Actual evapotranspiration, **(C)** Rainfall runoff, **(D)** Snowmelt. **(E)** Heat map for the long-term mean monthly distribution of rainfall runoff and snowmelt in each elevation band. **(F)** Percentage contribution from different flow components to the total discharge for sub-basins (given in the map) and Karnali basin overall (given in the legend).

seasonal water availability reduce the resilience of the basin in case of, for example, a failing monsoon. Overall, it is likely that the snow storage will decline, and the snowmelt season will shorten. For the Karnali basin, the snowmelt contribution to the overall discharge in the river is much higher than glacier melt.

4.3 Anomalies in discharge

We examined the interannual trends and monthly discharge deviations in the overall Karnali basin from 1991 to 2022 (Figure 6) and found both positive and negative anomalies. A notable negative anomaly was observed in October 2015, when the mean monthly discharge was approximately 50% lower than the long-term October mean. Negative discharge anomalies persisted for several consecutive months and extended through 2016. The El Niño event in 2015 could be the cause of the anomalies in precipitation and discharge. The annual precipitation in 2015 was 1,360 mm, which is less than the long-term average. However, ET remained close to the long-term average, explaining the deficit in the discharge. The following years, 2017 and 2018, were also characterized by dry summers. These persistent low discharge values across months and years can indicate the presence of a multiyear dry period.

Conversely, we detected several positive anomalies since 2019, indicating a multiyear wet period. The positive anomaly of 159% in October 2022 represents an extension of the wet period. These positive deviations are driven by the above-average annual precipitation received in the years 2019–2022. The discharge anomalies are also influenced by the onset, intensity and termination of monsoon rainfall, combined with higher snowmelt during those specific months. The study by Khanal et al. (2023) also highlights the increase in annual precipitation in the overall Ganges basin, to which the Karnali River is a major tributary. The occurrences of both extreme positive and negative anomalies within successive years highlight an increase in discharge variability.

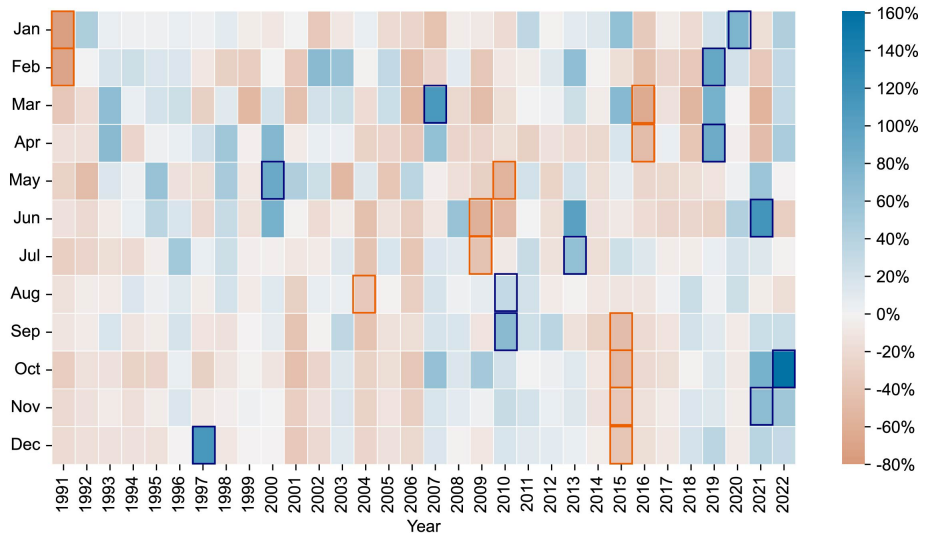

FIGURE 6
Heat map showing the monthly discharge deviation [%] from the long-term monthly average discharge in the Karnali basin overall for the period 1991–2022. The bounding box in orange and blue represents the driest and wettest months compared to the long-term average monthly discharge value of the study period.

4.4 Drought analysis

We identified the presence of dry and wet events in multiple years from the heat map in Figure 6. We quantified the severity of these events by calculating the meteorological (SPEI) and hydrological drought (SSI) indices for different aggregation periods. We then assessed the potentially lagged relationship between the climate drivers and streamflow response using cross-correlation. First, we tested different aggregation periods for the SPEI and SSI and quantified their correlation. We decided to use a 3-month aggregation period, which shows a high correlation and preserves short- term variability (Supplementary Figure A.5), a consideration important when analyzing the buffering capacity due to snow storage. We refer to these indices as SPEI-3 and SSI-3 for Karnali and its sub-basins. The highest correlation between SPEI and SSI was 0.74 (Figure 7A) with a lag time of 1 month. This indicated that the streamflow responded to the meteorological drought within a month.

Comparison of SPEI-3 and SSI-3 in Figure 8 showed the spread of drought period throughout the years in the basins. The magnitude and frequency of the droughts varied seasonally. In the overall Karnali basin, March had the highest number of hydrological drought events, and June had the lowest. On average, the mean duration of the hydrological dry periods was about 6 months for SSI < 0 for the period 1991 to 2022. Extreme droughts were mostly observed in pre-monsoon (MAM), post-monsoon (ON), and winter months (DJF). Major hydrological dry periods (drought index less than −1.5) were recorded in the years 2001–2002, 2004–2005, 2006–2007, 2009–2010, 2010–2011, and 2015–2017 in the overall Karnali basin, which correlated well with the occurrence of meteorological drought (see Figure 9C). These drought years were also identified by Khatiwada and Pandey (2019) in their study of droughts in Karnali. The occasional occurrence of hydrological drought in the monsoon period was observed in the years 2004, 2006, and 2009, out of which 2004 and 2006 were linked to multi-year drought events. In 2009, for example, precipitation was 12% lower than average. We observed the prevalence of similar hydrological drought events across the sub-basins, which indicates that drought in the monsoon of the year 2009 was driven by large-scale climate drivers. We also observed some extreme wet periods (SSI > 2) after 2019. These periods are consistent with above-average precipitation and ET (Supplementary Figures A.7, A.8).

In Figures 9A,B, we compared time series of precipitation, snow storage, and snowmelt against SSI values for the selected drought periods from 2004–2008 and 2014–2018 to understand the timing, behavior, and buffering of drought. In both periods, the precipitation deficit was the main driver of the hydrological drought in the basin. However, the onset and recovery of the droughts were influenced by the availability of snow storage. Annual precipitation, ET, and snowfall contribution are shown in Supplementary Figures A.6–A.8 to support the interpretation of the analysis.

During the first selected drought period from 2004 to 2008, we observed that the monthly snow storage is consistent with the precipitation (Figure 9A). In dry years like 2004 and 2006, the snow accumulation was also low, limiting snowmelt and prolonging the drought. Conversely, in 2005, high precipitation and associated snow storage across all elevation bands resulted in the recovery of a 12-month drought and flipped the SSI to a positive value. Snowmelt from areas below 5,000 m was also higher in the year 2005, which contributed to the drought recovery and maintained the pre-monsoon flow.

During the second selected drought period between 2014 and 2018, we observed higher snow storage even in the years with comparatively low precipitation and vice versa (Figure 9A). Although the total annual precipitation between the years from 2014 to 2018 was comparable (Supplementary Figure A.7), their monthly distributions were different. A nine-month-long drought recovered at the start of the year 2015 due to the combination of rainfall and higher snow storage below 5,000 m, contributing to the pre-monsoon melt. The higher snow storage above 5,000 m, buffered a new drought, and was delayed until September, even given anomalously low monsoon precipitation. We note that the snow

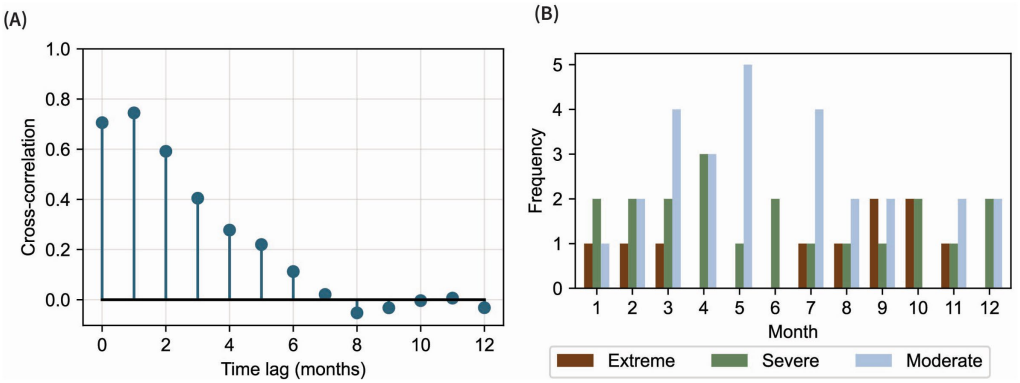

FIGURE 7
(A) Cross-correlations between SPEI-3 and SSI-3. **(B)** Monthly frequency distribution of hydrological drought occurrence based on SSI-3 indices categorized into moderate (–1 < SSI > –1.5), severe (–1.5 –<= SSI > –2.00), –and extreme (SSI < –2.00).

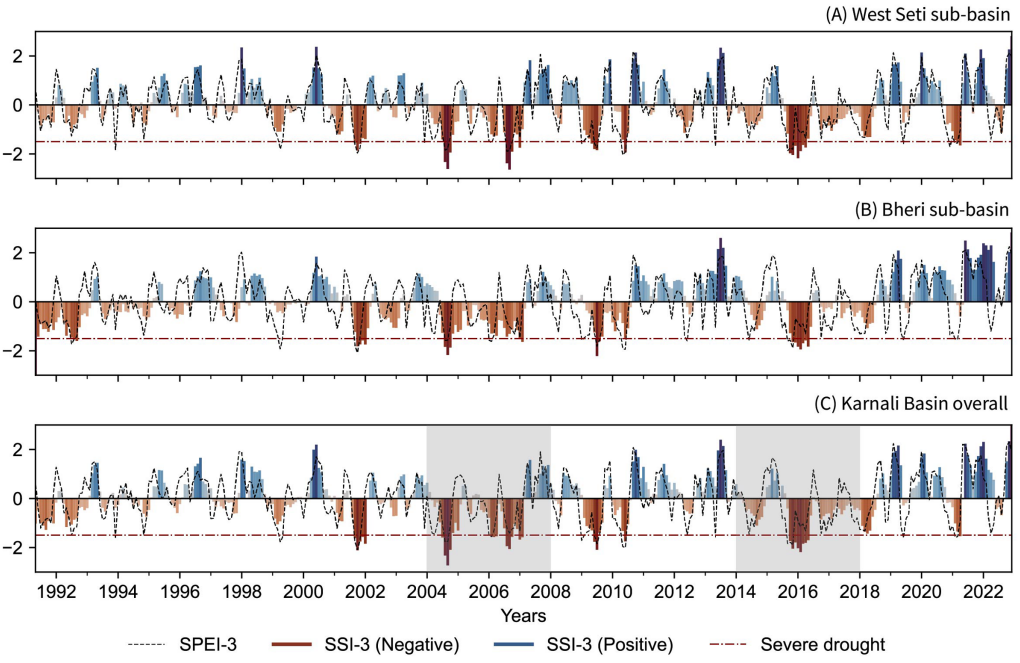

FIGURE 8
Comparison of the 3-month SPEI (line plot) and 3-month SSI (bar plot) with darker colors indicating higher categories of events, in sub-basins **(A,B)** and the Karnali basin overall **(C)**. The shading in Panel **(C)** highlights the selected drought years, which were studied in detail to understand the drought behavior.

storage in consecutive years was 50, 28 and 49% compared to the year 2015. This resulted in a multi-year, multi-season drought in consecutive years, lasting 24 months in total. Thus, a low snow storage could accelerate the propagation of meteorological drought to the onset of hydrological drought.

4.5 Drought buffering capacity due to snow storage

We tested the influence of initial snow storage, soil moisture, and baseflow on discharge variability at different locations in the basin. Our results showed that the initial baseflow and soil moisture conditions have a limited impact on discharge variability and the buffering of droughts. We therefore focused our analysis on the role of the initial snow storage. We compared the impact of initial snow storage and the impact of meteorological variability on the discharge variability (Figure 10). We showed that the initial snow storage has a substantial influence on discharge variability with the same order of magnitude as the meteorological variability. The snow storage impacts the discharge variability for several months. Only by August does this impact become negligible. The magnitude of the variability of discharge due to initial snow storage varies within the basin. For the outlets at higher elevation, the initial snow storage logically has a

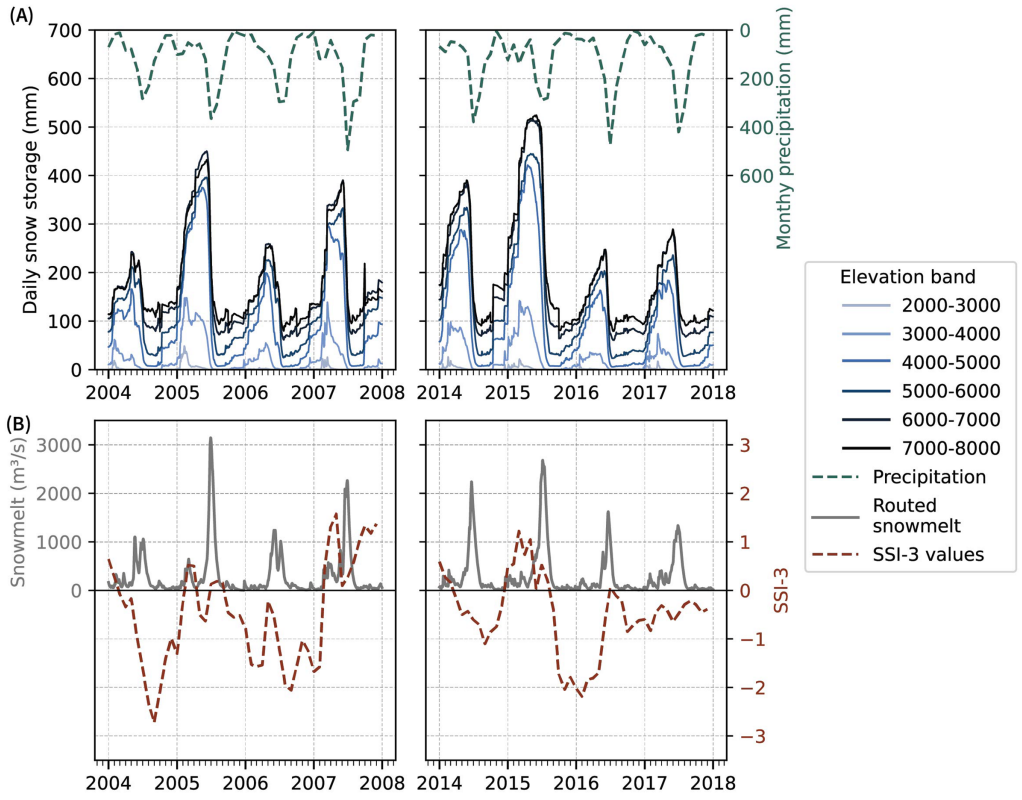

FIGURE 9
(A) Time series of daily snow storage (mm) at different elevation bands along with the monthly precipitation (mm) for the two selected drought periods. **(B)** Time series of daily routed snowmelt (m^3/s) corresponding to the index value of SSI-3 for the two selected drought periods.

larger control on discharge. For instance, at outlet G (2,137 m), we observed a CV of about 60% in the discharge during April–May and around 40% during July due to varying snow storage conditions. The first observed peak in CV was due to variability in snow storage below 5,000 m in the pre-monsoon, and the second peak was from variability in snow storage above 5,000 m. In contrast, for outlet A (186 m), the CV in discharge due to varying snow storage initial conditions was initially high but then decreased rapidly to 25%. This is still a considerable amount, but at the full basin scale, the variability in discharge was mostly controlled by meteorological variability. For short-term periods, the basin's resilience to droughts is largely influenced by the initial condition of the hydrological parameters. As time progresses, the impact of the initial hydrological condition decreases, and meteorological factors fully control discharge variability. This implies that as we move downstream, natural buffering capacity decreases and the flow regime becomes more controlled by meteorological variability. This indicates the need for integrated upstream downstream water management strategies including enhancing downstream storage system to strengthen drought buffering capacity.

5 Conclusion

In this study, we simulate the discharge of the Karnali basin to quantify the benchmark water balance components and assess drought response using the distributed hydrological model SPHY. We ran the model simulation for the reference period 1991–2022 at a high resolution of 500 meters using downscaled ERA5 meteorological data. The model performs well when compared to observations with KGE values ranging from 0.79 to 0.84 and average biases from −3.33 to 10.70%. A comparison between exceedance probabilities also shows good agreement.

The results of the model simulation were used to analyze the spatial and temporal patterns of contemporary hydrology and meteorology in the basin. Rain runoff is the major contributor to the total discharge, followed by baseflow and snowmelt for the Karnali basin overall. Our results show that the monthly distribution of water balance components within the sub-basins is comparable in timing but different in magnitude. The westerlies provide more precipitation in the west, and in particular, the West-Seti River sub-basin is the wettest and is characterized by a high rainfall runoff contribution. Snowmelt runoff peaks in June when the temperature is also at its maximum. Snowmelt runoff is highest in the upstream part of the Karnali basin, with most snowfall at higher elevations. Actual evapotranspiration peaks in July in the forested hill at intermediate elevations.

Our study demonstrates that both positive and negative monthly streamflow anomalies have been increasing over the last decade, which is indicative of more variable and less predictable streamflow regimes. The meteorological drought generally propagates to a hydrological drought with a lag of less than 1 month, and they are highly correlated. The onset and recovery of drought are influenced by the availability of snow. As snowmelt

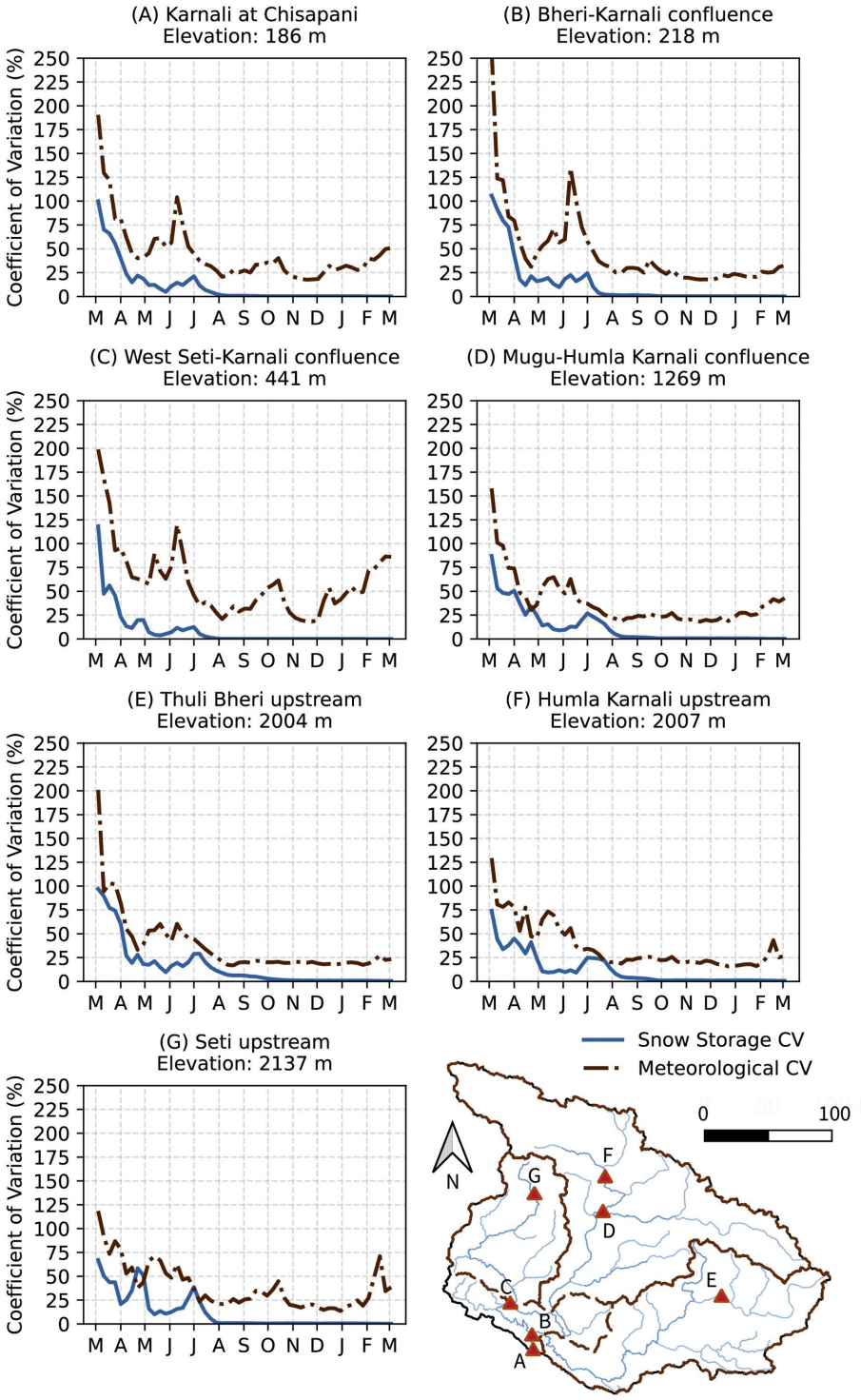

FIGURE 10
Coefficient of variance (CV) in the discharge for the outlets at different elevations (m) due to the initial condition of the snow storage and meteorological conditions as a function of time.

runoff plays a significant role in the total discharge in the basin, the variability in discharge is, for a considerable part, explained by the initial snow storage and therefore has an important buffering role. At higher elevations, lower discharge variability is observed, especially during the typical cold dry period, as the gradually melting snow acts as a natural buffer against drought. At lower elevations, streamflow relies mostly on rainfall and less on snowmelt, and this causes a high streamflow variability caused by meteorological conditions. A changing climate and shift in precipitation from snow to rain can impact the climate resilience of the Karnali considerably, therefore making the basin much more vulnerable to droughts in the future.

Data availability statement

The data supporting the conclusions of this article will be made available by the authors upon reasonable request. Restrictions apply to some datasets, including data obtained from the Department of Hydrology and Meteorology (DHM), which are subject to third-party permissions and cannot be shared publicly without authorization.

Author contributions

PP: Methodology, Formal analysis, Writing – original draft, Investigation, Data curation, Visualization, Resources, Writing – review & editing, Conceptualization. JG: Project administration, Supervision, Conceptualization, Writing – review & editing, Funding acquisition. TB: Funding acquisition, Supervision, Project administration, Writing – review & editing, Conceptualization. PK: Writing – review & editing, Methodology, Investigation. JF: Investigation, Writing – review & editing. WI: Investigation, Writing – review & editing, Conceptualization, Supervision, Funding acquisition, Methodology, Resources, Project administration.

Funding

The author(s) declared that financial support was received for this work and/or its publication. The authors of this research thank the Dutch Research Council NWO, with co-financing partners Planet, Rotterdam Zoo, Himalayan Tiger Foundation, and Practical Action, for funding the project Save the Tiger! Save the Grassland! Save the Water! (Grant No. NWA.1292.19.146) to which this research is part. The co-author, JF was supported by the Swiss National Science Foundation (Grant No. 179130).

Acknowledgments

We thank the Department of Hydrology and Meteorology Nepal, for making the measured hydrological and meteorological data available for this research. The authors are also thankful to Future Water (Wageningen, the Netherlands) for providing the source code for the SPHY model in the public domain.

Conflict of interest

The author(s) declared that this work was conducted in the absence of any commercial or financial relationships that could be construed as a potential conflict of interest.

Generative AI statement

The author(s) declared that Generative AI was not used in the creation of this manuscript.

Any alternative text (alt text) provided alongside figures in this article has been generated by Frontiers with the support of artificial intelligence and reasonable efforts have been made to ensure accuracy, including review by the authors wherever possible. If you identify any issues, please contact us.

Publisher's note

Supplementary material

The Supplementary material for this article can be found online at: https://www.frontiersin.org/articles/10.3389/frwa.2025.1720178/full#supplementary-material

References

Allen, R. G., Pereira, L. S., Raes, D., and Smith, M. (1998). FAO irrigation and drainage paper no. 56. Rome: Food and Agriculture Organization of the United Nations.

Armstrong, R. L., Rittger, K., Brodzik, M. J., Racoviteanu, A., Barrett, A. P., Khalsa, S.-J. S., et al. (2019). Runoff from glacier ice and seasonal snow in high Asia: separating melt water sources in river flow. *Reg. Environ. Chang.* 19, 1249–1261. doi: 10.1007/s10113-018-1429-0

Buri, P., Fatichi, S., Shaw, T. E., Miles, E. S., McCarthy, M. J., Fyffe, C. L., et al. (2023). Land surface modeling in the Himalayas: on the importance of evaporative fluxes for the water balance of a high-elevation catchment. *Water Resour. Res.* 59:e2022WR033841. doi: 10.1029/2022WR033841

Calvin, K., Dasgupta, D., Krinner, G., Mukherji, A., Thorne, P. W., Trisos, C., et al. (2023) in IPCC 2023: Climate change 2023: Synthesis report. contribution of working groups I, II and III to the sixth assessment report of the intergovernmental panel on climate change. eds. H. Lee and J. Romero (Geneva: Intergovernmental Panel on Climate Change (IPCC)).

Copernicus Climate Change Service (2019). Land cover classification gridded maps from 1992 to present derived from satellite observations. Bonn, Germany: Copernicus Climate Change Service (C3S) Climate Data Store (CDS). doi: 10.24381/cds.006f2c9a

Dahal, P., Shrestha, M. L., Panthi, J., and Pradhananga, D. (2020). Modeling the future impacts of climate change on water availability in the Karnali River basin of Nepal Himalaya. *Environ. Res.* 185:109430. doi: 10.1016/j.envres.2020.109430

Defourny, P., Lamarche, C., Brockmann, C., Boettcher, M., Bontemps, S., De Maet, T., et al. 2023 Observed annual global land-use change from 1992 to 2020 three times more dynamic than reported by inventory-based statistics, in preparation

Dhami, B., Himanshu, S. K., Pandey, A., and Gautam, A. K. (2018). Evaluation of the SWAT model for water balance study of a mountainous snowfed river basin of Nepal. *Environ. Earth Sci.* 77:21. doi: 10.1007/s12665-017-7210-8

Farinotti, D., Huss, M., Fürst, J. J., Landmann, J., Machguth, H., Maussion, F., et al. (2019). A consensus estimate for the ice thickness distribution of all glaciers on earth. *Nat. Geosci.* 12, 168–173. doi: 10.1038/s41561-019-0300-3

Fiddes, J., and Gruber, S. (2014). TopoSCALE v.1.0: downscaling gridded climate data in complex terrain. *Geosci. Model Dev.* 7, 387–405. doi: 10.5194/gmd-7-387-2014

Filhol, S., Fiddes, J., and Aalstad, K. (2023). TopoPyScale: a Python package for hillslope climate downscaling. *J. Open Source Softw.* 8:5059. doi: 10.21105/joss.05059

FutureWater. (2019). FutureWater/SPHY: Spatial Processes in HYdrology Hydrological Model. Avilable online at: https://github.com/FutureWater/SPHY/releases/tag/v3.0

Gobiet, A., Kotlarski, S., Beniston, M., Heinrich, G., Rajczak, J., and Stoffel, M. (2014). 21st century climate change in the European Alps—a review. *Sci. Total Environ.* 493, 1138–1151. doi: 10.1016/j.scitotenv.2013.07.050

Gupta, H. V., Kling, H., Yilmaz, K. K., and Martinez, G. F. (2009). Decomposition of the mean squared error and NSE performance criteria: implications for improving hydrological modelling. *J. Hydrol.* 377, 80–91. doi: 10.1016/j.jhydrol.2009.08.003

Hasan, M. A., and Pradhanang, S. M. (2017). Estimation of flow regime for a spatially varied Himalayan watershed using improved multi-site calibration of the soil and water assessment tool (SWAT) model. *Environ. Earth Sci.* 76:787. doi: 10.1007/s12665-017-7134-3

Hersbach, H., Bell, B., Berrisford, P., Hirahara, S., Horányi, A., Muñoz-Sabater, J., et al. (2020). The ERA5 global reanalysis. *Q. J. R. Meteorol. Soc.* 146, 1999–2049. doi: 10.1002/qj.3803

ICIMOD. (2021). Sub-sub-basins of Hindu Kush Himalaya (HKH) Region [Data set]. doi: 10.26066/RDS.7952

Immerzeel, W. W., Lutz, A. F., Andrade, M., Bahl, A., Biemans, H., Bolch, T., et al. (2020). Importance and vulnerability of the world's water towers. *Nature* 577, 364–369. doi: 10.1038/s41586-019-1822-y

Immerzeel, W. W., Pellicciotti, F., and Bierkens, M. F. P. (2013). Rising river flows throughout the twenty-first century in two Himalayan glacierized watersheds. *Nat. Geosci.* 6, 742–745. doi: 10.1038/ngeo1896

Immerzeel, W. W., van Beek, L. P. H., and Bierkens, M. F. P. (2010). Climate change will affect the Asian water towers. *Science* 328, 1382–1385. doi: 10.1126/science.1183188

Ishida, K., Ohara, N., Ercan, A., Jang, S., Trinh, T., Kavvas, M. L., et al. (2019). Impacts of climate change on snow accumulation and melting processes over mountainous regions in northern California during the 21st century. *Sci. Total Environ.* 685, 104–115. doi: 10.1016/j.scitotenv.2019.05.255

Japan Aerospace Exploration Agency, (2021). ALOS world 3D 30 meter DEM. V3.2. Distributed by open topography. Tokyo: Japan Aerospace Exploration Agency. doi: 10.5069/G94M92HB

Khanal, S., Lutz, A. f., Kraaijenbrink, P. D. A., van den Hurk, B., Yao, T., and Immerzeel, W. W. (2021). Variable 21st century climate change response for rivers in High Mountain Asia at seasonal to decadal time scales. *Water Resour. Res.* 57:e2020WR029266. doi: 10.1029/2020WR029266

Khanal, S., Tiwari, S., Lutz, A. F., Hurk, B. V. D., and Immerzeel, W. W. (2023). Historical climate trends over High Mountain Asia derived from ERA5 reanalysis data. *J. Appl. Meteorol. Climatol.* 62:45. doi: 10.1175/JAMC-D-21-0045.1

Khanal, S., Lutz, A. F., Eekhout, J., Terink, W., Aubry-Wake, C., and Immerzeel, S. (2024). SPHY v3.1: Spatial Processes in Hydrology. Model theory, installation, and data preparation. *FutureWater Report* 248:124. Available online at: https://futurewater.gitbook.io/sphy-manual

Khatakho, R., Talchabhadel, R., and Thapa, B. R. (2021). Evaluation of different precipitation inputs on streamflow simulation in Himalayan River basin. *J. Hydrol.* 599:126390. doi: 10.1016/j.jhydrol.2021.126390

Khatiwada, K. R., and Pandey, V. P. (2019). Characterization of hydro-meteorological drought in Nepal Himalaya: a case of Karnali River basin. *Weather Clim. Extremes* 26:100239. doi: 10.1016/j.wace.2019.100239

Khatiwada, K. R., Panthi, J., Shrestha, M. L., and Nepal, S. (2016). Hydro-climatic variability in the Karnali River basin of Nepal Himalaya. *Climate* 4:17. doi: 10.3390/cli4020017

Kraaijenbrink, P. D. A., Bierkens, M. F. P., Lutz, A. F., and Immerzeel, W. W. (2017). Impact of a global temperature rise of 1.5 degrees Celsius on Asia's glaciers. *Nature* 549, 257–260. doi: 10.1038/nature23878

Kraaijenbrink, P. D. A., Stigter, E. E., Yao, T., and Immerzeel, W. W. (2021). Climate change decisive for Asia's snow meltwater supply. *Nat. Clim. Chang.* 11, 591–597. doi: 10.1038/s41558-021-01074-x

Lalande, M., Ménégoz, M., Krinner, G., Naegeli, K., and Wunderle, S. (2021). Climate change in the High Mountain Asia in CMIP6. *Earth Syst. Dynam.* 12, 1061–1098. doi: 10.5194/esd-12-1061-2021

Lavers, D. A., Simmons, A., Vamborg, F., and Rodwell, M. J. (2022). An evaluation of ERA5 precipitation for climate monitoring. *Q. J. R. Meteorol. Soc.* 148, 3152–3165. doi: 10.1002/qj.4351

Lutz, A. F., Immerzeel, W. W., Kraaijenbrink, P. D. A., Shrestha, A. B., and Bierkens, M. F. P. (2016). Climate change impacts on the upper Indus hydrology: sources, shifts and extremes. *PLoS One* 11:e0165630. doi: 10.1371/journal.pone.0165630

Lutz, A. F., Immerzeel, W. W., Shrestha, A. B., and Bierkens, M. F. P. (2014). Consistent increase in high Asia's runoff due to increasing glacier melt and precipitation. *Nature Clim. Change* 4, 587–592. doi: 10.1038/nclimate2237

McKee, T. B., Doesken, N. J., and Kleist, J. (1993). The relationship of drought frequency and duration to time scales 8th Conference on Applied Climatology, Anaheim, 17-22 January 1993, 179–184.

Modarres, R. (2007). Streamflow drought time series forecasting. *Stoch. Environ. Res. Risk Assess.* 21, 223–233. doi: 10.1007/s00477-006-0058-1

Musselman, K. N., Clark, M. P., Liu, C., Ikeda, K., and Rasmussen, R. (2017). Slower snowmelt in a warmer world. *Nature Clim. Change* 7, 214–219. doi: 10.1038/nclimate3225

Nash, J. E., and Sutcliffe, J. V. (1970). River flow forecasting through conceptual models part I — a discussion of principles. *J. Hydrol.* 10, 282–290. doi: 10.1016/0022-1694(70)90255-6

Nepal, J., Pant, R. R., Shrestha, S., Paudel, S., Bishwakarma, K., Awasthi, M. P., et al. (2024). Water balance estimation and runoff simulation of Chameliya watershed, Nepal. *Environ. Earth Sci.* 83:117. doi: 10.1007/s12665-024-11430-7

Pandey, V. P., Dhaubanjar, S., Bharati, L., and Thapa, B. R. (2020a). Spatio-temporal distribution of water availability in Karnali-Mohana Basin, Western Nepal: hydrological model development using multi-site calibration approach (Part-A). *J. Hydrol. Reg. Stud.* 29:100690. doi: 10.1016/j.ejrh.2020.100690

Pandey, V. P., Dhaubanjar, S., Bharati, L., and Thapa, B. R. (2020b). Spatio-temporal distribution of water availability in Karnali-Mohana Basin, Western Nepal: Climate change impact assessment (Part-B). *J Hydrol. Reg. Stud.* doi: 10.1016/j.ejrh.2020.100691

Pandey, V. P., Sharma, A., Dhaubanjar, S., Bharati, L., and Joshi, I. R. (2019). Climate shocks and responses in Karnali-Mahakali basins, Western Nepal. *Climate* 7:92. doi: 10.3390/cli7070092

Peña-Gallardo, M., Vicente-Serrano, S. M., Hannaford, J., Lorenzo-Lacruz, J., Svoboda, M., Domínguez-Castro, F., et al. (2019). Complex influences of meteorological drought time-scales on hydrological droughts in natural basins of the contiguous unites states. *J. Hydrol.* 568, 611–625. doi: 10.1016/j.jhydrol.2018.11.026

Pervez, M. S., and Henebry, G. M. (2015). Assessing the impacts of climate and land use and land cover change on the freshwater availability in the Brahmaputra River basin. *J. Hydrol. Reg. Stud.* 3, 285–311. doi: 10.1016/j.ejrh.2014.09.003

Pfeffer, W. T., Arendt, A. A., Bliss, A., Bolch, T., Cogley, J. G., Gardner, A. S., et al. (2014). The Randolph glacier inventory: a globally complete inventory of glaciers. *J. Glaciol.* 60, 537–552. doi: 10.3189/2014JoG13J176

Pradhan, A. M. S., Silwal, G., Shrestha, S., Huynh, T.-C., and Dawadi, S. (2024). Can a spatially distributed hydrological model effectively analyze hydrological processes in the Nepal Himalaya River basin? *Environ. Model. Assess.* 29, 1037–1058. doi: 10.1007/s10666-024-09975-9

Pradhananga, S., Nepal, S., Kamal, S. K., and Hafeez, M. (2025). Climate change will exacerbate seasonal flow variability in the Karnali River basin: implications for water, energy, and agriculture sectors. *Hydrol. Res.* 56, 471–491. doi: 10.2166/nh.2025.193

Ragettli, S., Cortés, G., McPhee, J., and Pellicciotti, F. (2014). An evaluation of approaches for modelling hydrological processes in high-elevation, glacierized Andean watersheds. *Hydrol. Process.* 28, 5674–5695. doi: 10.1002/hyp.10055

Ragettli, S., Immerzeel, W. W., and Pellicciotti, F. (2016). Contrasting climate change impact on river flows from high-altitude catchments in the Himalayan and Andes Mountains. *Proc. Natl. Acad. Sci.* 113, 9222–9227. doi: 10.1073/pnas.1606526113

Ragettli, S., Pellicciotti, F., Immerzeel, W. W., Miles, E. S., Petersen, L., Heynen, M., et al. (2015). Unraveling the hydrology of a Himalayan catchment through integration of high resolution in situ data and remote sensing with an advanced simulation model. *Adv. Water Resour.* 78, 94–111. doi: 10.1016/j.advwatres.2015.01.013

Raje, D., Priya, P., and Krishnan, R. (2014). Macroscale hydrological modelling approach for study of large scale hydrologic impacts under climate change in Indian river basins. *Hydrol. Process.* 28, 1874–1889. doi: 10.1002/hyp.9731

RGI Consortium (2017). Randolph glacier inventory - a dataset of global glacier outlines, version 6 [data set]. Boulder: National Snow and Ice Data Center.

Simons, G.W.H., Koster, R., and Droogers, P. 2020 HiHydroSoil v2.0 - high resolution soil maps of global hydraulic properties. Wageningen, The Netherlands.

Srivastava, S., Azam, M. F., and Thakur, P. K. (2024). Linking basin-scale hydrology with climatic parameters in western Himalaya: application of satellite data, temperature index modelling and in-situ observations. *Geosci. Front.* 15:101936. doi: 10.1016/j.gsf.2024.101936

Terink, W., Lutz, A. F., Simons, G. W. H., Immerzeel, W. W., and Droogers, P. (2015). SPHY v2.0: spatial processes in HYdrology. *Geosci. Model Dev.* 8, 2009–2034. doi: 10.5194/gmd-8-2009-2015

UNEP-WCMC. (2026). Protected Area Profile for Nepal from the World Database on Protected Areas [WWW Document]. Protected Planet. Avilable online at: https://www.protectedplanet.net/country/NPL (Accessed May 2, 2026).

Van Loon, A. F., Tijdeman, E., Wanders, N., Van Lanen, H. a. J., Teuling, A. J., and Uijlenhoet, R. (2014). How climate seasonality modifies drought duration and deficit. *J. Geophys. Res. Atmos.* 119, 4640–4656. doi: 10.1002/2013JD020383

Vicente-Serrano, S. M., Beguería, S., and López-Moreno, J. I. (2010). A multiscalar drought index sensitive to global warming: the standardized precipitation evapotranspiration index. *J. Clim.* 23:909. doi: 10.1175/2009JCLI2909.1

Vicente-Serrano, S. M., López-Moreno, J. I., Beguería, S., Lorenzo-Lacruz, J., Azorin-Molina, C., and Morán-Tejeda, E. (2012). Accurate computation of a streamflow drought index. *J. Hydrol. Eng.* 17, 318–332. doi: 10.1061/(ASCE)HE.1943-5584.0000433

Viviroli, D., Dürr, H. H., Messerli, B., Meybeck, M., and Weingartner, R. (2007). Mountains of the world, water towers for humanity: typology, mapping, and global significance. *Water Resour. Res.* 43:653. doi: 10.1029/2006WR005653

Viviroli, D., Kummu, M., Meybeck, M., Kallio, M., and Wada, Y. (2020). Increasing dependence of lowland populations on mountain water resources. *Nat. Sustain.* 3, 917–928. doi: 10.1038/s41893-020-0559-9

Wanders, N., Thober, S., Kumar, R., Pan, M., Sheffield, J., Samaniego, L., et al. (2019). Development and evaluation of a Pan-European multimodel seasonal hydrological forecasting system. *J. Hydrometeorol.* 20:40. doi: 10.1175/JHM-D-18-0040.1

Wang, S., Yan, M., Yan, Y., Shi, C., and He, L. (2012). Contributions of climate change and human activities to the changes in runoff increment in different sections of the Yellow River. *Quat. Int.* 282, 66–77. doi: 10.1016/j.quaint.2012.07.011

Wijngaard, R. R., Biemans, H., Lutz, A. F., Shrestha, A. B., Wester, P., and Immerzeel, W. W. (2018). Climate change vs. socio-economic development: understanding the future south Asian water gap. *Hydrol. Earth Syst. Sci.* 22, 6297–6321. doi: 10.5194/hess-22-6297-2018

Wijngaard, R. R., Lutz, A. F., Nepal, S., Khanal, S., Pradhananga, S., Shrestha, A. B., et al. (2017). Future changes in hydro-climatic extremes in the upper Indus, Ganges, and Brahmaputra River basins. *PLoS One* 12:e0190224. doi: 10.1371/journal.pone.0190224

Yoon, Y., Kumar, S. V., Forman, B. A., Zaitchik, B. F., Kwon, Y., Qian, Y., et al. (2019). Evaluating the uncertainty of terrestrial water budget components over High Mountain Asia. *Front. Earth Sci.* 7:120. doi: 10.3389/feart.2019.00120

Zhang, T., Li, D., and Lu, X. (2022). Response of runoff components to climate change in the source-region of the Yellow River on the Tibetan plateau. *Hydrol. Process.* 36:e14633. doi: 10.1002/hyp.14633